Numerical modelling of the light-hole exciton diamagnetic shift and g-factor in GaAs/AlGaAs quantum wells.

M. A. Chukeev and P. S. Grigoryev
Spin Optics Laboratory, St. Petersburg State University, Ulyanovskaya 1, Peterhof, St. Petersburg, 198504, Russia

S. A. Eliseev, V. A. Lovtcius, and Yu. P. Efimov
Resource Center "Nanophotonics", St. Petersburg State University, Ulyanovskaya 1, Peterhof, St. Petersburg, 198504, Russia

(Dated: October 6, 2022)

Light-hole excitons in quantum wells are less studied than the heavy-hole ones. In this paper, we focus on the observation of the light-hole exciton behavior in the GaAs/AlGaAs quantum well in the presence of the external magnetic field. We analyze the behaviour in terms of g-factor and a diamagnetic shift constant. These values were extracted from the reflectance spectra obtained in magnetic field up to $B = 6\,\mathrm{T}$. To model experimental results a numerical approach solving the multidimensional Schroedinger equation is employed. It accounts for the heavy-hole-light-hole coupling according to Luttinger Hamiltonian. Comparison with experiment revealed surprisingly low diamagnetic shift in experiment with diamagnetic constant $\varkappa = 3.37 \times 10^{-5}\,\mathrm{eV/T^2}$. A series of calculations was conducted varying problem parameters to reveal the origin of the low diamagnetic shift. A further development of the numerical technique is needed to fully describe the behavior of the light-hole exciton.

INTRODUCTION

Light hole exciton states in QWs have remained untackled by the researchers[1–5] in comparison to the heavy-hole ones[6–12]. The reason is twofold. On one hand, the heavy-hole exciton state in the GaAs-based heterostructures lies lower in energy, therefore it is observable in both reflectance and photoluminescence spectra. Unlike the light-hole exciton, which has roughly threefold less oscillator strength and effective channel of relaxation to the heavy-hole exciton state. On the other hand, their properties are far too similar to address less available to the experimental observations light hole state. On top of that exciton states in quasi-two-dimensional structures present difficulties to theoretical description, in particular, due to the penetration of quasiparticles into the barrier, interplay of Coloumb coupling with QW potential, and, finally, heavy-hole-light-hole (hh-lh) coupling in the GaAs-based heterostructures.

Modern computation capabilities allow one to effectively solve the Schroedinger equation for the exciton in the QW taking into account all the above mentioned peculiarities of the system. Numerical calculations of exciton states has been developed for some time now[11–16] and several aspects of the exciton behavior have been successfully described in that studies. Exciton binding energy, its oscillator strength across various QW widths, the g-factor renormalization were modelled in the framework of the numerical calculation.

Theoretical studies of the light-hole (lh) properties in the QW heterostructures rely on the Luttinger-Kohn model[17,18]. The situation in the QW is particularly interesting for the ground lh state in the QW as it is in the close vicinity of the second state of size quantization for the heavy hole (hh). One would expect, that varying QW width or the AlGaAs barrier height the properties of the light hole can vary dramatically due to the hh-lh coupling. However the formation of the exciton complicates all sorts of theoretical efforts in this system. We attempt to resolve this problem by means of the numerical calculation.

Experimental studies of the lh exciton g-factor were conducted previously[19–21]. They showed lh g-factor variation with QW width. Study [19] presents measurements in which lh g-factor remains larger than 6, while in study [21] this value is strictly lower than 6 for all studied QWs. Possible reason for this difference lies in composition of the studied samples, which shows sensitivity of the g-factor to the QW potential parameters. To model these g-factor variations one has to take into account the hh-lh coupling.

We also address the experimental aspect of the lh exciton study. We use reflectance spectroscopy technique with separate detection of two opposite circular polarizations. In experiment external magnetic field spans from 0 to 6 T, with the sample placed in cryostat at $T = 1.5\,\mathrm{K}$. Our access to the heterostructure samples of the high-cristalline quality results in the reliable experimental results. To verify the quality of the heterostructure we resort to the reflectance characterisation of the grown samples. It allows one to determine radiative, Γ_0, and nonradiative, Γ, broadenings of the exciton resonance, thus introducing a numerical value of the heterostructure quality in form of their ratio $q = \Gamma_0/\Gamma$. This value represents ratio of excitons emitted light to those scattered from the exciton state to other channels of relaxation, in some structures in can be close to unity. In our present work we measured lh exciton state in a 14-nm GaAs/AlGaAs QW in presence of the external magnetic field up to $B = 6\,\mathrm{T}$ by means of reflectance spectroscopy.

In the studied sample value q reaches 0.1 for lh exciton and 0.3 for the hh one.

The manuscript is arranged as follows: first we present the methods that we used in our study, then in section II we discuss our numerical results in comparison to the experimental data, we complete our study in discussion section followed by the conclusions.

I. METHODS

A. Experiment

Experiment uses reflectance spectroscopy of the specially selected MBE-grown sample of fine crystalline quality. The sample was grown on [001] substrate, and contains a 14-nm GaAs QW surrounded by AlGaAs barriers with Al concentration of 3 %.

In experiment the light from incandescent lamp, passed through 100 μm pin-hole and fell on the sample at normal incidence. The sample was cooled to $T = 1.5$ K in a cryostat, equipped with a split coil superconducting magnet, providing magnetic field up to $B = 6$ T in Faraday geometry. Light spot on the sample has the size of about 100 μm. The reflected beam is then put into the detection system which consists of the $\lambda/4$ zero order wave plate and a Glan-Taylor prism to separate circular polarizations. The detection is performed by the CCD-array, attached to a 0.5-meter monochromator with gratings of 1200 gr./mm.

Only one lens was placed near the magnet coils to focus the incident beam and collect the reflected one. It had nonmagnetic mounting to avoid light beam alternation with magnetic field applied. All other optical elements were placed more than 2 meters away from the cryostat. Due to geometrical limitation of the setup the light beams were rotated. Special effort was made to preserve the polarisation of the reflected beam, it was redirected by two prisms, using full internal reflection twice, so the polarisation distortion that appears at each reflection would cancel out.

Reflectance spectra obtained in this measurements are shown in figure 1. the hh exciton state and the lh exciton states are found at positions expected in the 14-nm GaAs-based QW. These energy positions are subject to size-quantization effect and Coloumb binding effect acting in opposite directions. Size quantization is expected to shift lh exciton higher due to the smaller mass, while Coloumb attraction is weaker in case of the lh exciton due to smaller reduced mass.

The hh exciton state is accompanied with the low intensity peak approximately 1 meV lower in energy, which we ascribe to the trion state, and a similar in amplitude peak that clearly has different from the hh exciton g-factor of unknown nature. Possibly it is the dark exciton state that somewhat interacts with light due to hh-lh coupling. The hh exciton state and the lh one exhibit diamagnetic shift and Zeeman splitting. In the GaAs based QWs exciton Zeeman splitting is subject to the renormalization which we investigated in detail for wider QWs[15]. From this previous experience we attepmpt to describe Zeeman splitting and diamagnetic shift using the numerical calculation.

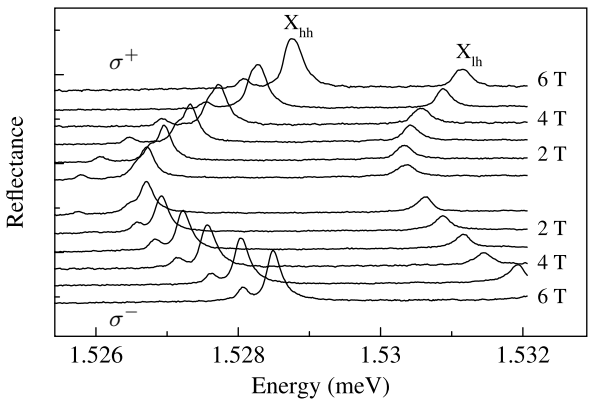

FIG. 1. Reflectance spectrum of heterostructure T670 with the 14-nm GaAs/$Al_{0.03}Ga_{0.97}As$ QW. Labels "X_{hh}" and "X_{lh}" mark the exciton states of hh and lh excitons. Magnetic field was applied in Faraday geometry, detection is separate for the opposite circular polarizations.

B. Calculation

Details of our numerical approach were already presented in our earlier studies[15]. It is based on the finite difference method for solving Schrödinger equation. The Hamiltonian is represented in form of a matrix, which eigenvectors are the numerical values of the wave function on the given grid. The eigenvalues of the matrix are approximations of the energies of the exciton states.

The Hamiltonian employed in this study has general form:

$$\hat{H} = \hat{H}_c + \hat{H}_v - \frac{e^2}{\varepsilon\sqrt{\rho^2+(z_e-z_h)^2}} + V_{\mathrm{QW}}(z_e, z_h) - 2\kappa J\mu_B B - \sigma g_e \mu_B B \quad (1)$$

here ε is the dielectric constant, e is electron charge, $z_{e,h}$ are the coordinates of the electron/hole along the growth axis, and ρ is the relative electron-hole distance in the QW plane. Term V_{QW} represents independent square QW potentials for electron and hole and two last terms represent the energy of the magnetic momenta J and σ in the external magnetic field B with coefficients g_e and 2κ, that take into account renormalization of valence band and conduction band g-factors due to interaction with distant bands in crystal. For GaAs $g_e = -0.44$[22,23] and $\kappa = -1.2$. The minus sign in the last two terms represents that usually collinear to magnetic field momenta have smaller energy than anticollinear.

The kinetic term $\hat{H}_c$ for the conduction band is defined by the single effective electron mass, $m_e = 0.0067m_0$:

$$\hat{H}_c = -\frac{\hbar^2 \hat{k}_e^2}{2m_e} \tag{2}$$

For the valence band, however, we use Luttinger Hamiltonian, which uses three parameters γ_1, γ_2, and γ_3 to describe the distortion of the valence band by the cubic crystalline potential. To simplify the Hamiltonian we shift to the center-of-mass and polar relative coordinates in the QW plane. This transformation together with generalized $\hat{k}_{e,h}$ operators leads to massive expressions[15]. Transition to the polar relative coordinates allows to extract quantum number k_φ, which is valid for the diagonal part of the Luttinger Hamiltonian. The diagonal elements of the Hamiltonian acquire a from:

$$\begin{aligned}(H_c + H_v)_{\text{diag}} = & -\tfrac{\hbar^2}{2\mu_{xy}}\left(\tfrac{1}{\rho}\tfrac{\partial}{\partial\rho}\left(\rho\tfrac{\partial}{\partial\rho}\right) - \tfrac{k_\varphi^2}{\rho^2}\right) \\ & - \tfrac{\hbar^2}{2m_{hz}}\tfrac{\partial^2}{\partial z_h^2} - \tfrac{\hbar^2}{2m_e}\tfrac{\partial^2}{\partial z_e^2} \\ & + \tfrac{\rho^2}{2\mu_{xy}}\left(\tfrac{eB}{2c}\right)^2 - k_\varphi \tfrac{e\hbar B}{2c}\left(\tfrac{m_h - m_e}{M\mu_{xy}}\right)\end{aligned} \tag{3}$$

The first two lines represent the kinetic energy of the relative motion in the QW plane and along the growth direction for the electron and hole separately, third line describes the diamagnetic shift and energy correction for the exciton orbital momentum in magnetic field.

Yet the diagonal part of the Luttinger Hamiltonian presents itself in the chosen sets of coordinates as shown in expressions (1, 3), however, nondiagonal elements of the Hamiltonian alter the cylindrical symmetry, thus for the whole Hamiltonian of the problem the k_φ quantum number is not applicable. Here we resign to the simplification that quantum number k_φ defines a set of solutions for the diagonal part of the Hamiltonian, and nondiagonal elements describe interaction between several such sets, according to the selection rules arising from the cubic symmetry of the Hamiltonian.

According to this approach we compose a restricted Hamiltonian that includes operator (1) for $k_\varphi = 0$,1, and ± 2. Thus we consider optically active states of the diagonal part of the Hamiltonian ($k_\varphi = 0$), and those sets of solutions that primarily couple with the optically active exciton states. A restricted Hamiltonian therefore has the following form:

$$\hat{H} = \begin{pmatrix} H_{\text{hh},k_\varphi=0} & H_{12} & H_{13} & H_{13} \\ H_{21} & H_{\text{lh},k_\varphi=1} & 0 & 0 \\ H_{31} & 0 & H_{\text{lh},k_\varphi=2} & 0 \\ H_{31} & 0 & 0 & H_{\text{lh},k_\varphi=-2} \end{pmatrix} \tag{4}$$

This structure represents a restricted Hamiltonian employed to describe optically active hh exciton state, while for the lh exciton the indexes denoting the hole mass would be reverted. Indexes "hh" and "lh" correspond to substitution of hh and lh effective masses into expression (3). In particular:

$$m_{\text{hh},z} = \frac{m_0}{\gamma_1 - 2\gamma_2} \tag{5}$$

$$m_{\text{lh},z} = \frac{m_0}{\gamma_1 + 2\gamma_2} \tag{6}$$

$$m_{\text{hh},xy} = \frac{m_0}{\gamma_1 + \gamma_2} \tag{7}$$

$$m_{\text{lh},xy} = \frac{m_0}{\gamma_1 - \gamma_2} \tag{8}$$

Operators $H_{12,21}$ and $H_{13,31}$ follow from the Luttinger Hamiltonian. $H_{12,21}$ couple the heavy holes with the light hole with same sign of angular momentum projection on z-axis, while operators $H_{13,31}$ couple those with opposite ones. The detailed description of these operators is given in [15].

For the Hamiltonian described above we set the grid in z_e, z_h, and ρ coordinates. The grid should be large enough to comprise the exciton wave function, but fine enough to accurately represent square QW potential and, more importantly, Coloumb potential. For a region along ρ coordinate where ρ exceeds exciton Bohr radius the uniform grid is dramatically inefficient since the wave function is mainly exponentially decays in this region. Therefore we introduced a nonuniform grid according to a technique used in paper by Liu *et al.*[24]. Appendix contains particular functions defining grid node coordinates, that we used in our calculation.

II. COMPARISON

We have performed the calculations of the exciton energies and their wave functions with nominal parameters of our heterostructure. Namely QW width $L = 14\,\text{nm}$, the Al concentration in barriers was 3%, which corresponds to $V_c + V_v = 42\,\text{meV}$ of the barrier height. We used $V_e/V_v = 67/33$ ratio, and mass parameters were $m_e = 0.0665$, $\gamma_1 = 6.98$, $\gamma_2 = 2.06$, $\gamma_3 = 2.9$ according to the recommendation of the paper by Vurgaftman *et al.*[25].

Figure 2 compares our results to the experimentally obtained data. Dashed line corresponds to the calculated hh exciton energies in the 14-nm QW. The lh exciton energies for this calculation are not shown to avoid cluttering of the figure as they fall on the experimental resonances of the hh exciton.

To match the energy position of the exciton state we varied the QW width and found that for $L_{\text{QW}} = 11.35$ the calculation almost coincides with the experimental data (blue and red connected dots). In spite this good agreement the diamagnetic shift in experiment is still less pronounced. Difference in diamagnetic shift is particularly prominent for the lh exciton. One can consider this as an indicator that experimental behaviour of the lh exctiton state corresponds to more compact exciton state.

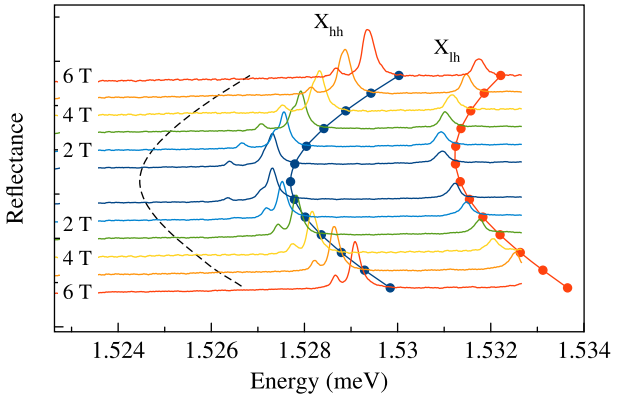

FIG. 2. Reflectance spectra in comparison with calculation at nominal parameter (dashed line), and with calculation with QW width set to $L_{\mathrm{QW}} = 11.35\,\mathrm{nm}$ (blue and red connected dots). Light blue dots correspond to the lh exciton position extracted from nonradiative broadening excitation spectra. For the nominal parameter calculation only hh curve is shawn, because lh curve overlays the experimental spectra.

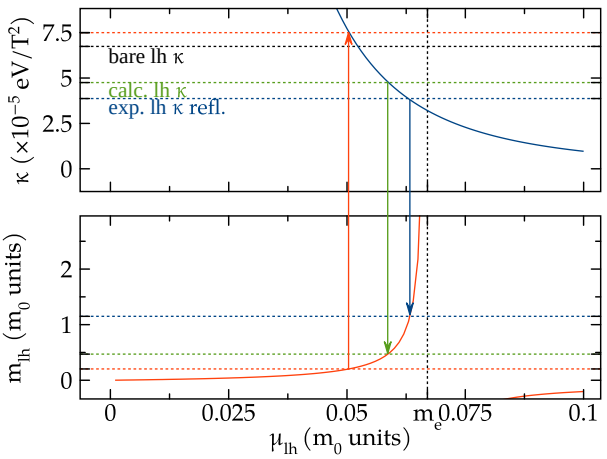

FIG. 3. Diamagnetic shift constant as function of the reduced mass in isotropic approximation (9) (top panel), and lh effective mass as a function of the reduced mass (bottom panel)

Indeed hydrogen-like exciton state in bulk material would have diamagnetic shift that is presented by the formula:

$$\Delta E_{\mathrm{diam}} = \frac{\langle\rho\rangle^2 e^2}{8c^2\mu} B^2 = \frac{2\pi^2\varepsilon^2\hbar^2}{c^2\mu^3 e^2} B^2 \qquad (9)$$

this expression uses Bohr exciton radius as mean value of electron-hole distance perpendicular to the magnetic field direction, $\langle\rho\rangle$. To reduce this value one have to reduce dielectric constant ε, thus reducing screening of the charges in the medium, or increase the reduced mass μ. Since the dielectric constant of GaAs is easily measured via reflectance, its value is reliable. Therefore we consider an increase of the reduced mass μ. In particular, by the increase of the lh mass. Figure 3 shows isotropic lh mass as a function of the reduced mass of the exciton in its bottom panel. When one considers bare lh mass as in Eq. (8) formula (9) gives diamagnetic constant value highlighted by the red arrow in the figure. It is close to the value obtained in our numerical calculation without accounting for the hh-lh coupling (black dashed line denoted "bare lh κ"). Deviation from our calculation is explained by the anisotropy of the diagonal part of the exciton Hamiltonian. When we consider diamagnetic constant retrieved from our calculation and from the experiment (green and blue dashed lines correspondingly), the reduced mass is increased so that isotropic lh mass is of about $0.5m_0$ for the calculation and as high as m_0 for the experimental data. This brings us to the conclusion that (a) hh-lh coupling is responsible for the low value of the diamagnetic shift of the lh exciton, and (b) observed discrepancy between calculated diamagnetic constant for the lh exciton and that measured experimentally is significant and requires further investigation.

In particular, hh-lh coupling can provide lh with a negative effective mass in the vicinity of Γ point. If the wave vector of the lh confined in the exciton would be distributed close to this point in the inverse space, the reduced mass can increase even further. Although such fine tuning of the heterostructure parameters is hardly can be achieved for the real-life samples, our numerical model can ignore the growth technology limitations.

III. DISCUSSION

We conducted several attempts to reach the coupling regime in which the lh subband would acquire negative mass near the Γ point. Those include varying V_c/V_v ratio, accounting for additional hh-lh coupling due to symmetry breaking on the boarders of the QW, and variation of the Luttinger parameters in the vicinity of their recommended values. To compare various calculation results to experimental values we fitted the lh exciton energy positions as function of magnetic field by the formula:

$$E_{\mathrm{ex}}(B) = E_0 - \frac{1}{2} g\mu_B B + \kappa B^2 \qquad (10)$$

here we introduced mean exciton g-factor, g, and diamagnetic constant, κ. Experimental values appeared to be $g = 3.9$, $\kappa = 3.87 \times 10^{-5}\,\mathrm{eV/T^2}$. Here we use term mean g-factor due to slight deviation of the exciton energy splitting from the linear dependency. It arises from hh-lh coupling variation with the magnetic field increase.

Our first approach lies in varying V_e/V_h ratio. The underlying idea is to tune the energy distance between the observable lh exciton state and those dark hh exciton states that couple to it, and thus enhance the coupling to acquire lower diamagnetic shift constant. Figure 4(a) presents g-factors and diamagnetic constants obtained in

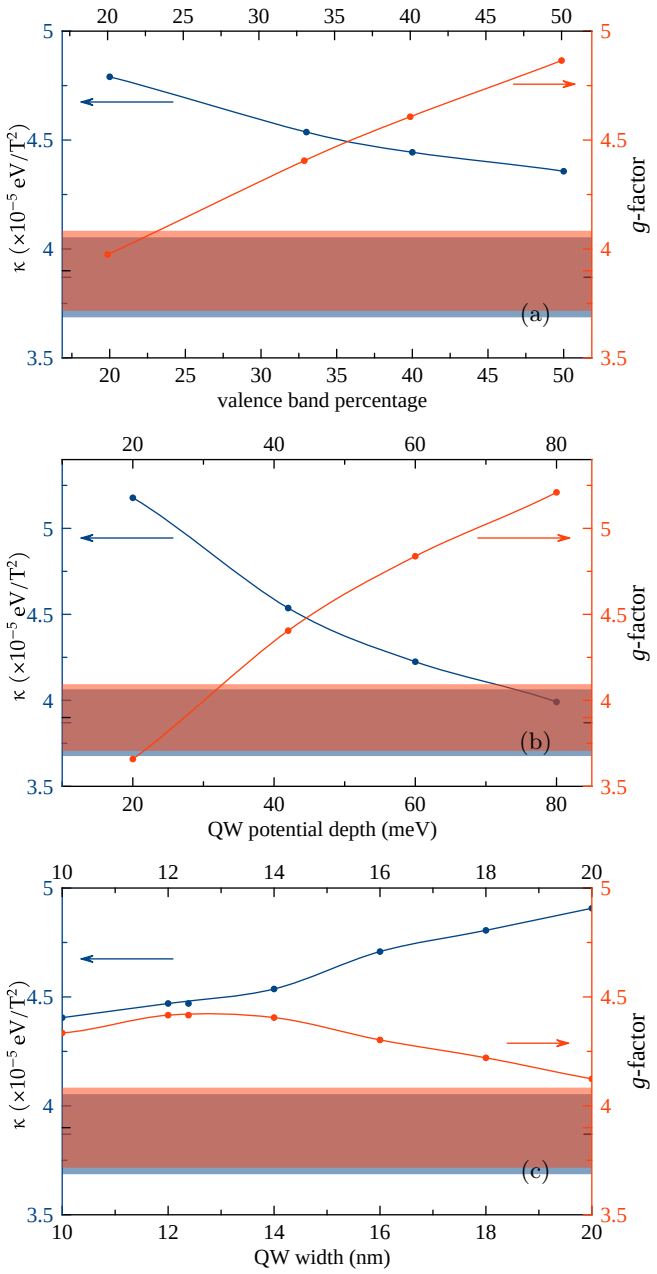

FIG. 4. The mean g-factor (red) and the diamagnetic constant (blue) values as a function of the valence band share in the overall QW potential depth (a), the depth of the QW potential (b), and the QW width (c). Red and blue stripes show values extracted from the experiment, the width of the stripe represents the uncertainty in the experimental value.

calculation as a function of the QW depth share in the valence band. One can clearly see that although increase in the valence band share leads to the decrease in the diamagnetic constant, the g-factor, in turn, tends to worse agreement with the experiment. Furthermore, calculations with variation of the QW depth and of the QW width also confirmed the opposite trends in g-factor and κ behavior (see Figs 4 (b) and (c)). This correlation of g-factor and κ clearly shows that no variation of QW potential parameters can lead to simultaneous agreement of both parameters with the experiment. As we have shown in figure 2, setting QW width to $L_{\mathrm{QW}} = 11.35\,\mathrm{nm}$ brings calculated energies in agreement with experimentally measured ones. Although calculations in figure 4 (a) and (b) were done for the nominal 14-nm QW width, still lower QW width corresponds to great agreement for the g-factor, and significant deviation for the diamagnetic constant. Yet, given that calculation of the bare g and κ (without hh-lh coupling) have values 2.8 and $6.7 \times 10^{-5}\,\mathrm{eV/T^2}$, the agreement is strikingly good, especially for the g-factor value.

These figures illustrate that the decrease of the lateral exciton size, required to achieve experimental value of κ, is not easily obtained by the QW potential variation. In particular we examine higher QW depths and lower QW widths, such variations enhance exciton localization. Deeper QW leads to localization of charge carriers in the growth direction, thus enhancing their Coloumb coupling. Decreasing QW width acts in a similar manner. This logic indeed works to a certain extent, however the decrease of κ while deepening the QW or decreasing it width is not enough even for the unrealistically high QW potential depth.

Next we considered accounting for the additional hh-lh coupling which occurs due to the symmetry breaking on the QW border locally reducing the crystalline symmetry. Based on the paper by M. Durnev *et al.*[18] this hh-lh coupling introduces addition to the Hamiltonian:

$$\hat{H}_{\mathrm{add}} = \frac{t_{\text{l-h}}\hbar^2}{\sqrt{3}m_0 a_0}\left\{J_x, J_y\right\}\left(\delta(z_h - z_l) + \delta(z_h - z_r)\right) \quad (11)$$

here a_0 is the lattice constant, $t_{\text{l-h}}$ is the constant of about unity, figure brackets denote anticommutator of the hole angular momentum matrices J_x and J_y, and z_l,z_r are left and right QW border coordinate respectively. Since we are unable to introduce a delta-function into our numerical calculation, we replaced it with a Gaussian curve with parameter:

$$\delta(x) \leftrightarrow \frac{1}{\delta x}\frac{e^{-\frac{x}{\delta x}}}{\left(e^{-\frac{x}{\delta x}}+1\right)^2} \quad (12)$$

we used $\delta x = 0.258\,\mathrm{nm}$ value in the calculation, which corresponds to the half of the lattice constant of the GaAs. Once we introduced term (11) to our calculation we calculated κ and g parameters for various values of $t_{\text{l-h}}$. Results are shown in figure 5

It appears that our substitution of the delta-function by the Gaussian curve gives rise to a significant effect even for rather small values of parameter $t_{\text{l-h}}$. Though we achieve the desired regime, when the g-factor remains almost unchanged while the κ changes significantly, the additional coupling leads to the increase of the diamagnetic shift constant.

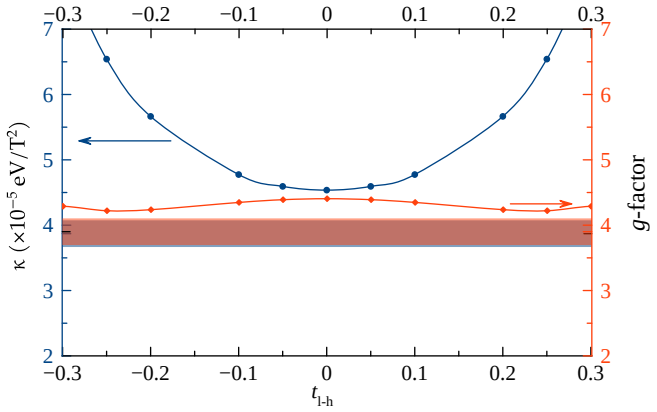

FIG. 5. The mean g-factor (red) and the diamagnetic constant (blue) values as a function of the $t_{\text{l-h}}$ parameter. Dashed grid lines show values extracted from the experiment.

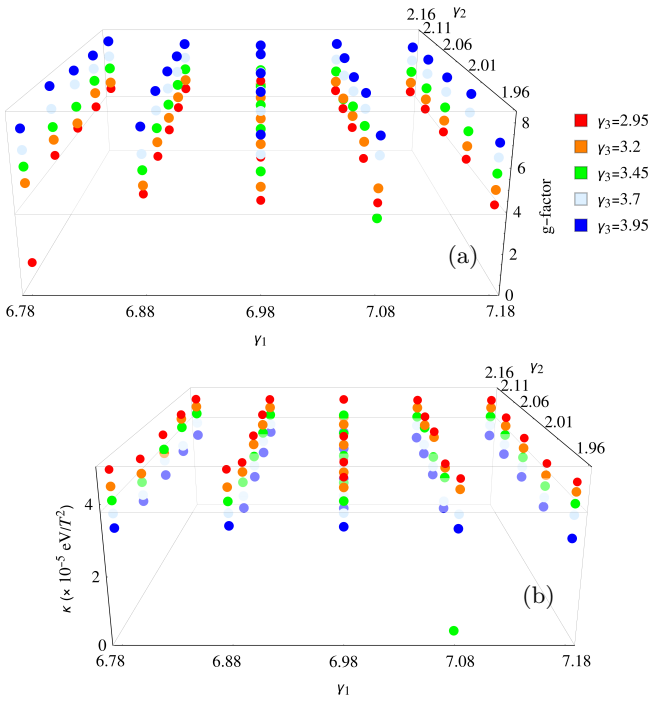

FIG. 6. The g-factor values (a) and the diamagnetic constant values of the lh exciton (b) as a function of the Luttinger parameters γ_1, γ_2, and γ_3. Colors correspond to various values of γ_3 parameter.

We assume that our substitution of the delta-function overestimates the effect of the additional symmetry-driven coupling, since the original paper[18] uses value $t_{\text{l-h}} = 0.5$. On the other hand, calculations in that paper considered $Al_{0.3}Ga_{0.7}As/GaAs$ QWs, with much higher barriers, than in our case of tenfold less 3 % Al content in the barriers.

Finally we produced a series of calculations for varying Luttinger parameters γ_1, γ_2, and γ_3. We varied parameters in the vicinity of the recommended parameters. Figure 6 represents the results of calculations.

Clearly, slight variation near the recommended values has little effect on the diamagnetic constant and g-factor. And even though hh-lh coupling decreases κ for ever increasing γ_3, g-factor in that case tends to increase. Variation of γ_1 and γ_2 has only slight effect on both parameters. Varying Luttinger parameters we could not reach the desired experimental values of κ and g. However agreement achieved in our calculation is remarkable. Indeed, we conducted calculation without hh-lh coupling and found that bare lh exciton g-factor is $g_{\text{bare}} = 2.84$, and bare diamagnetic constant value was found to be $\kappa_{\text{bare}} = 6.74 \times 10^{-5}\,\text{eV/T}^2$.

We have considered calculation of the lh exciton g-factor and diamagnetic constant and tested a large set of various parameters in attempt to reach a better agreement with experiment. Though used Luttinger parameters provide great agreement between numerical computation and experiment, further experimental verification on a large set of samples as well as further numerical analysis is required to refine the set of parameters for GaAs based heterostructures.

IV. CONCLUSION

Experimental reflectance measurements showed surprisingly low diamagnetic shift of the lh exciton state in the 14-nm QW with 3% Al content. To explain this behaviour we employed a numerical technique of solving Schrödinger equation based on the finite difference method. The technique accounts for the hh-lh coupling using Luttinger Hamiltonian, and allows one to examine exciton states behavior under the influence of external magnetic field in Faraday geometry.

We found a significant deviation of the calculated diamagnetic shift value from the experimentally observed one. Several approaches were undertaken to converge calculation results to the experimentally observed values of g-factor and diamagnetic constant. We analysed an effect of bands mismatch ratio, depth of the QW, and QW width on the parameters. We also analysed possible effect of the additional symmetry-driven hh-lh coupling on the parameters. This additional coupling comes from breaking of the crystalline symmetry at the QW boundaries. It could not however explain the deviation of our model from the experimental data.

Finally we varied Luttinger parameters γ_1, γ_2, and γ_3, and found no significant improvement in the agreement with experiment of calculated values g and κ, however parameters obtained in our calculation are already close to the experimental values. We suggest that further development of the numerical model can lead to even better agreement.

ACKNOWLEDGMENTS

Financial support from the Russian Science Foundation, grant No. 21-72-00037, is acknowledged. The authors acknowledge Saint-Petersburg State University for a research grant 91182694. The authors also thank Recourse Center "Nanophotonics" SPbU for the heterostructures studied in the present work and A. Levantovsky for the software "MagicPlot" extensively used for the data analysis.

Appendix A: Numerical procedure for the hh-lh mixing

To optimize calculation time we implemented nonuniform grid in our calculation domain to decrease the number of grid nodes. In our previous study[15] we modelled relatively wide QW with width of 95 nm. Using the uniform grid we used grid $n_e \times n_h \times n_\rho = 70 \times 70 \times 200$ in a $120 \times 120 \times 400\,\mathrm{nm}^3$ domain. The large size of domain alonr the ρ coordinate is required to accurately describe exponentially decaying exciton wave function. Here n_e and n_h are the numbers of nodes along the z_e and z_h direction, respectively, and n_ρ is that along the ρ direction. When one implements nonuniform grid number of nodes in such domain can be reduced to $60\times60\times60$ points shrinking the matrix almost eightfold by dimension. This allowed us to add hh-lh coupling into consideration. In this study all calculations were made on $60 \times 60 \times 60$ grid in $50 \times 50 \times 160\,\mathrm{nm}^3$ domain.

The non-uniform grid is defined by the polynomial smooth piecewise functions, defining coordinates of the nodes:

$$z_i = \begin{cases} ih_z + \left(\left(i-5-\frac{n}{2}\right)^3 - \left(5-\frac{n}{2}\right)^3\right) l_z, \text{if } i > \frac{n}{2}+5 \\ ih_z, \text{if } \left|i-\frac{n}{2}\right| < 5 \\ ih_z + \left(\left(i+5-\frac{n}{2}\right)^3 - \left(5-\frac{n}{2}\right)^3\right) l_z, \text{if } i < \frac{n}{2}-5 \end{cases} \quad \text{(A1)}$$

$$\rho_i = \begin{cases} ih_\rho, \text{if } i < 8 \\ ih_\rho + (i-8)^3 l_\rho, \text{if } i \geq 8 \end{cases} \quad \text{(A2)}$$

where h_z, l_z, h_ρ and l_ρ are constants, defining the scale of linear and nonlinear parts of the grid, $n = n_e = n_h$ is the number of nodes along z coordinate (in current calculations $h_\rho = 0.66\,\mathrm{nm}$, $l_\rho = 2.3 \times 10^{-4}\,\mathrm{nm}$, $h_z = 0.66\,\mathrm{nm}$, $l_z = 3.5 \times 10^{-4}\,\mathrm{nm}$). Constants 5 and 8 were arbitrary chosen. Function (A1) was used for z_e and z_h coordinates.

Difference schemes for the nonuniform grid were made similarly to the schemes in Ref.[24]. For the schemes not present in that paper, a Tailor series expansion was employed to construct system of linear equations, defining scheme coefficients. We used the schemes with accuracy not worse than $\mathcal{O}(h^2)$, where h is characteristic distance between nodes. Particular form of the differential operators were taken following the[15], where similar problem was solved for a wide InGaAs/GaAs QW.

It should be noted that, taking coupling into account demands high accuracy from the calculation. Indeed, the wave functions of states with angular momentum 1, that get mixed to the ground exciton states, have two zeros along the ρ axis. To describe such functions accurately, one has to use grids with smaller step size in the vicinity of the $\rho = 0$ point. In our calculation, step less than 1 nm was required to achieve reliable results. On the other hand in the region of higher ρ values, the wave function tends to the exponential decay. It does not oscillate, but having in mind zero boundary conditions in the calculation, it is necessary to set larger domain in the ρ direction. Step size in this region can be larger. Our nonuniform grid approach meets both these requirements, and allows one to reliably calculate the exciton wave function.

[1] W. T. Masselink, P. J. Pearah, J. Klem, C. K. Peng, and H. Morkoç, Absorption coefficients and exciton oscillator strengths in A1GaAs-GaAs superlattices, Phys. Rev. B **32**, 8027 (1985).

[2] R. T. Collins, L. Viña, W. I. Wang, L. L. Chang, and L. Esaki, Mixing between heavy-hole and light-hole excitons in GaAs/Al_xGa_{1-x}As quantum wells in an electric field, Phys. Rev. B **36**, 1531 (1987).

[3] B. Gil, Y. El Khalifi, H. Mathieu, C. de Paris, J. Massies, G. Neu, T. Fukunaga, and H. Nakashima, Line-shape analysis of the refiectivity spectra of GaAs/(Ga, A1)As single quantum wells grown on (001)- and (311)-oriented substrates, Phys. Rev. B **41**, 2885 (1990).

[4] D. K. Loginov, E. V. Ubyivovk, Yu. P. Efimov, V. V. Petrov, S. A. Eliseev, Yu. K. Dolgikh, I. V. Ignatiev, V. P. Kochereshko, and A. V. Selkin, Interference of polariton waves in structures with wide GaAs/AlGaAs quantum wells, Fiz. Tverd. Tela **48**, 1979 (2006) [Phys. Solid State **48**, 2100 (2006)].

[5] P. Yu. Shapochkin, S. A. Eliseev, V. A. Lovtcius, and Yu. P. Efimov, P. S. Grigoryev, E. S. Khramtsov, and I. V. Ignatiev, Excitonic probe for quantum-state engineering by MBE technology, Phys. Rev. Applied **12**, 034034 (2019).

[6] R. Dingle, W. Wiegmann, and C. H. Henry, Quantum States of Confined Carriers in Very Thin AlGaAs-GaAs-AlGaAs Heterostructures, Phys. Rev. Lett. **33**, 827 (1974).

[7] B. Deveaud, F. Clèrot, N. Roy, K. Satzke, B. Sermage, and D. S. Katzer, Phys. Rev. Lett. **67**, 2355 (1991).

[8] E. L. Ivchenko, *Optical Spectroscopy of Semiconductor Nanostructures* (Springer, Berlin 2004).

[9] L. C. Andreani, Solid State Commun. **77**, 641 (1991).

[10] A. V. Trifonov, S. N. Korotan, A. S. Kurdyubov, I. Ya. Gerlovin, I. V. Ignatiev, Yu. P. Efimov, S. A. Eliseev, V. V. Petrov, Yu. K. Dolgikh, V. V. Ovsyankin, and A. V. Kavokin, Phys. Rev. B **91**, 115307 (2015).

[11] E. S. Khramtsov, P. A. Belov, P. S. Grigoryev, I. V. Ig-

natiev, S. Yu. Verbin, Yu. P. Efimov, S. A. Eliseev, V. A. Lovtcius, V. V. Petrov, and S. L. Yakovlev, Radiative decay rate of excitons in square quantum wells: Microscopic modeling and experiment, J. Appl. Phys. **119**, 184301 (2016).

[12] P. S. Grigoryev, A. S. Kurdyubov, M. S. Kuznetsova, I. V. Ignatiev, Yu. P. Efimov, S. A. Eliseev, V.V. Petrov, V.A. Lovtcius, P.Yu. Shapochkin, Superlattices and Microstructures **97**, 452 (2016).

[13] E. S. Khramtsov, P. S. Grigoryev, D. K. Loginov, I. V. Ignatiev, Yu. P. Efimov, S. A. Eliseev, P. Yu. Shapochkin, E. L. Ivchenko, and M. Bayer, Exciton spectroscopy of optical reflection from wide quantum wells, Phys. Rev. B **99**, 035431 (2019).

[14] P. A. Belov, Energy spectrum of excitons in square quantum wells, Phys. E, **112**, 96 (2019).

[15] P. S. Grigoryev, O. A. Yugov, S. A. Eliseev, Yu. P. Efimov, V. A. Lovtcius, V. V. Petrov, V. F. Sapega, and I. V. Ignatiev, Inversion of Zeeman splitting of exciton states in InGaAs quantum wells, Phys. Rev. B **93**, 205425 (2016).

[16] P. S. Grigoryev, V. G. Davydov, S. A. Eliseev, Yu. P. Efimov, V. A. Lovtcius, P. Yu. Shapochkin, I. V. Ignatiev, and M. Bayer, Exciton-light coupling in (In,Ga)As/GaAs quantum wells in longitudinal magnetic field, Phys. Rev. B **96**, 155404 (2017).

[17] I. L. Aleiner, E. L. Ivchenko, Anisotropic exchange splitting in type-II GaAs/AlGaAs superlattices, Pis'ma Zh. Eksp. Teor. Fiz. 55 (1992) 662 (transl: JETP Letters 55 (1992) 692).

[18] M.V. Durnev, M.M. Glazov, E.L. Ivchenko, Giant Zeeman splitting of light holes in GaAs/AlGaAs quantum wells, Phys. E, **44**, 797 (2012)

[19] A. Arora, A. Mandal, S. Chakrabarti,and S. GhoshJ., Magneto-optical Kerr effect spectroscopy based study of Lande g-factor for holes in GaAs/AlGaAs single quantum wells under low magnetic fields, Appl. Phys., **113**, 213505 (2013).

[20] V. B. Timofeev, M. Bayer, A. Forchel & M. Potemski, Mixing of excitonic states containing light and heavy holes in an isolated GaAs/AlGaAs quantum well in a magnetic field, JETP Lett., **64**, 57 (1996).

[21] Y. H. Chen, X. L. Ye, B. Xu, Z. G. Wang, and Z. Yang, Large g-factors of higher-lying excitons detected with reflectance difference spectroscopy in GaAs-based quantum wells, Appl. Phys. Lett., **89**, 051903 (2006).

[22] L. M. Roth, B. Lax, and S. Zwerdling, Phys. Rev. 114, 90 (1959)

[23] I. A. Yugova, A. Greilich, D. R. Yakovlev, A. A. Kiselev, M. Bayer, V. V. Petrov, Y. K. Dolgikh, D. Reuter, and A. D. Wieck, Phys. Rev. B 75, 245302 (2007).

[24] J. Liu, G. A. Pope, K. Sepehrnoori, A high resolution finite-difference scheme for nonuniform grids, Appl. Math. Modeling **19**, 162 (1995)

[25] I. Vurgaftman, J. R. Meyer, and L. R. Ram-Mohan, Band parameters for III-V compound semiconductors and their alloys, J. Appl. Phys. **89**, 5815 (2001).